

Analysis, Design, and Testing of Airfoils for Use at Ultra-Low Reynolds Numbers

Peter J. Kunz
Ilan M. Kroo

Abstract:

Advances in technology have begun to make ultra-low Reynolds number flight a real possibility. The growing interest in vehicle development has created a need for an improved understanding of the relevant aerodynamics. A reasonable starting point is the study of airfoil section aerodynamics at ultra-low Reynolds numbers.

General effects on performance of several geometry characteristics of two-dimensional airfoils are explored using an incompressible Navier-Stokes solver. Reynolds numbers considered are 10,000 or less and the flow-field is assumed to be fully laminar. Variations in the thickness, camber, and leading/trailing edge shape are considered. Initial results indicate an increase in the maximum lift coefficient with decreasing Reynolds number. The lift to drag ratio decreases over this same range, but for certain applications, the ability to generate lift is a primary constraint on feasibility.

The associated drag corresponds to increased power requirements or reduced endurance. Neither option is desirable, but detailed airfoil section design for these Reynolds numbers offers a partial solution. The small body of experimental work has utilized simple plates or existing low-speed airfoil sections. Contrary to the notion that most sections perform similarly at ultra-low Reynolds numbers, the computational results indicate that the detailed section geometry still has a profound effect on airfoil performance. Improved section performance requires that the overall section thickness should be minimized, but the camber distribution also appears to have a strong influence. To explore the design space, the flow-solver has been coupled with an optimizer. The results of the optimization study indicate that unconventional camberlines may offer significant performance gains.

Application of a computational tool to this new flight regime dictates the need for some form of validation. The scaling difficulties eliminate most conventional methods of airfoil testing. The experimental method currently being developed involves the manufacture of micro-gliders for flight testing in still air. Performance estimates for these vehicles have been developed using the computed two-dimensional section properties and conventional aircraft performance calculations. The measured flight performance will provide good indication of the accuracy of the computational results.

Introduction:

The flight regime of micro-aircraft poses difficulties for aerodynamic analysis and design, but little experimental or computation work exists for aerodynamic surfaces operating at very low Reynolds numbers. Technological advances in micro-fabrication techniques and in the miniaturization of electronics are beginning to make mechanical micro-flight vehicles feasible from a systems and manufacturing standpoint. Very small devices can now be built and there are numerous potential application for these vehicles, but first they must be capable of flight. The reduced scale and low flight speeds of these vehicles result in Reynolds numbers on the order of

10^3 . Although insects have been flying happily under these conditions for quite some time, this is a new flight environment for man-made aircraft.

Aerodynamics at these Reynolds numbers are considerably different from those of more conventional aircraft. The flow is laminar and viscously dominated. Boundary layers are quite thick, often reaching a significant fraction of the chord length. Flow separation is an issue, even at low angles of attack. There is considerable literature on biological flight mechanisms, but there is very little detailed aerodynamic research available. The study of flight under these conditions is only now becoming more than an academic problem. A lack of suitable manufacturing technologies, the absence of sophisticated computational analysis methods, and the difficulties associated with accurate experimental work at this scale have restricted research in this area. Advances in technology have reduced the significance of the first two issues, but experimental work remains problematic. A reasonable solution is proposed in this paper.

A study of two-dimensional airfoil geometry is a reasonable starting point for exploration. The parameters investigated include thickness, camber, and leading and trailing edge shapes. The airfoil sections are analyzed using a two-dimensional, incompressible, Navier-Stokes solver. The flow field is assumed to be fully laminar.

Compared to performance at higher Reynolds numbers, the study demonstrates an order of magnitude increase in the drag and a similar sized reduction in lift to drag ratios. Although the drag rapidly increases with reductions in Re , significant lift coefficients are still attainable. Within the $Re 10^3$ range, reducing the Reynolds number results in an *increase* in the maximum steady-state lift. As Reynolds number is lowered, there is an alleviation of the leading edge suction peak which results in less adverse gradients along the low-pressure side of the airfoil. This delays separation and allows operation at higher angles of attack.

Examination of the geometry parameters reveals several trends. There is an expected drag penalty associated with increased thickness, but also a significant reduction in the lift curve slope. An additional increment in the pressure recovery, due to thickness, degrades the lifting performance and results in an earlier onset of separation. Given the benefits of reduced airfoil thickness, the remaining studies utilize 2% thick geometries. The performance of these thinner airfoils appears to be insensitive to the thickness distribution, but the magnitude and distribution of camber are still highly effective parameters. Building on the results of the geometry survey, several sections have been developed using an automated optimization method. Maximizing the two-dimensional lift to drag ratio at a given Reynolds number is the design goal.

Validation of the computational results will consist of experimental flight testing of small gliders. These tiny aircraft are constructed with a specific airfoil of interest and designed to achieve a steady-state glide at a defined Reynolds number. This is full-scale flight testing at a very small size. Estimates of the aircraft's performance have been developed using the results of the two-dimensional section analyses. Comparison of the predicted performance with flight test data will provide a good assessment of the accuracy of the two-dimensional computational results.

Computational Analysis Methods:

The computational analyses make extensive use of the INS2D two-dimensional incompressible Navier-Stokes solver developed by Rogers.^{1,2} This code utilizes the artificial compressibility method, first introduced by Chorin.³ RANS solvers generally require some form of preconditioning to solve very low Mach number flows. As the Mach number is decreased, the flow field approaches the incompressible limit. In this limit, the conservation of mass becomes an elliptic relation for a homogeneous flow. The acoustic wave speed, the dominant speed of propagation within the computational domain, becomes infinite. Fundamentally, hyperbolic flow solvers are not well suited to elliptic problems.

The artificial compressibility method offers a straightforward and efficient means of preconditioning to allow for the solution of an incompressible homogeneous flow field. The incompressible conservation of mass equation, an elliptic Laplace equation,

$$\partial_j u_j = 0 \quad (1)$$

is modified by the addition of a pseudo-time derivative of density.

$$\partial_\tau \rho + \partial_j u_j = 0 \quad (2)$$

Density is related to pressure via an artificial equation of state, where δ is the artificial compressibility.

$$p = \rho / \delta \quad (3)$$

This introduces an artificial and finite acoustic speed governed by the selection of the δ parameter. This addition to the conservation of mass equation, combined with the conservation of momentum equation, results in a hyperbolic system of equations which may be marched in pseudo-time. As the solution converges to a steady state, the artificial compressibility term drops out and a divergence-free solution is attained. The artificial compressibility is seen to act similarly to a relaxation parameter.

Using integral boundary layer formulations in conjunction with inviscid flow field solutions offers the potential for significant computational savings over viscous flow solvers. The MSES program developed by Drela⁴ has been implemented with limited success. This is a two-dimensional Euler solver, coupled with an integral boundary layer formulation. It appears to give reasonable drag predictions over a narrow range of angle of attack, but the limitations of the boundary layer formulation cause the solution to diverge if significant regions of separated flow exist. This is a general limitation of these methods. Unfortunately, this is often the case with airfoils operating in this regime, even at moderate angles of attack. This code also faces low

Mach number limitations like the compressible Navier-Stokes solvers, but has converged for Mach numbers as low as 0.15.

A comparison of results from MSES and INS2D for NACA 4402 and NACA 4404 airfoils at Re 1000 are presented in Figures 1 and 2. The upper end of each curve represents the maximum angle of attack for which a steady-state solution was attainable. The most obvious feature is the failure of the MSES analysis at about 3 degrees geometric angle of attack, much earlier than the INS2D results, which continue to converge past 10 degrees. Over the range in which MSES does converge to a solution, the trends in the results agree well with the INS2D calculations, and drag values are close, although the curves appear offset to some degree. In both figures, the effects of increasing thickness agree. Both analyses indicate similar reductions in the lift curve slope and equivalent increases in drag. The MSES solutions predict a lower lift curve slope and a slightly higher α_{ZL} , resulting in a significant deviation in predicted lift, and approximately 5% lower drag than the equivalent INS2D results. These results indicate that under the limitations of low angles of attack, the much faster inviscid/integral boundary layer codes provide a functional alternative to full viscous flow field solutions, but would not be applicable for detailed design, where analysis of the entire operating range is needed.

Flow Field Assumptions:

The analyses make use of three assumptions about the flow field. The flow is incompressible by the formulation of the flow solver, the flow is fully laminar, and the flow field is steady. The assumption of incompressibility is well justified for this application. The highest Mach number encountered in an associated vehicle development program was 0.3, and this was at the tip of a small 2 centimeter diameter rotor spinning at over 40,000 RPM. For a broad range of applications the Mach number will be considerably below this value and essentially incompressible.

The justification of the fully laminar flow assumption is more uncertain, but seems reasonable for the Reynolds numbers and geometries of interest. In the absence of separation, the flow will be entirely laminar. Even slight to moderate separation will likely result in laminar reattachment for chord Reynolds numbers below 10,000 on a smooth airfoil. The degree of separation which might result in transition and the transition length are the unclear issues. The alternatives are even less agreeable. The flow field could be assumed fully turbulent, which is surely not the case, or transition could be artificially and rigidly imposed at a specified location. Of these three, the fully laminar assumption appears to be the least restrictive and most physically accurate.

The steady-state assumption represents tremendous computational savings over time-accurate analysis. Airfoil polars have been generated by incrementally increasing the angle of attack until the steady-state solution failed to converge. Analyses were completed at Reynolds numbers of 1000, 2000, 6000, and 12,000. For analyses at Re 6000 and above, failure to converge is taken as an indication of unsteady phenomena in the flow field. This method appears to be reasonable and conservative for the flow regime and geometries of interest. For the lower

Reynolds number cases, lack of convergence can only be used as a definitive indicator if the overall convergence rate is slowed considerably. For the Re 1000 and Re 2000 cases, the polars have been computed assuming a steady-state flow field, but then a time accurate analysis has been completed at or above the indicated maximum lift to drag ratio angle of attack. This assures the absence of significant unsteady effects in the presented data, but does not represent a rigidly defined upper limit. It is possible that higher angles of attack would still exhibit steady behavior.

The steady-state results for an NACA 4402 airfoil at Re 6000 have been compared with data generated using the time-accurate mode of INS2D. The results of this study are illustrated in Figures 3 and 4. The time accurate computations represent an impulsive start with 20 chord lengths of total travel. Each time step represents 0.02 chord lengths of travel. The steady-state solutions are represented by the horizontal reference lines in the figures. The markers on the 8 degrees case represent the results from a halving of the time step. These demonstrate that the 0.02 chord length time step is adequate for resolution of the temporal variations. Steady-state analysis failed to converge at 5 degrees geometric angle of attack. Time accurate solutions agree with the steady-state result up past 4 degrees angle of attack. At six degrees, one degree past the point where the steady state analysis stops, small amplitude periodic behavior is visible. The lift and drag of the section are still reasonably well defined. At eight degrees, the amplitude of the oscillations has increased considerably and multi-frequency shedding is visible.

The results of these time accurate computations at higher angles of attack indicate that much higher lift coefficients may be attainable within the unsteady range of operation. Although inviting, these operating points would be difficult to exploit in practice. The increase in lift comes at the cost of a very large increase in drag. In this case, an increase in angle of attack from 4.0 to 8.0 degrees results in more than double the drag, to an average value of over 1000 counts. Although the percentage increase in drag from zero to four degrees is roughly the same, the rise in drag is doubled. This large penalty in the drag, combined with the time variation of section performance, limits the utilization of these unsteady operating points.

Effects of Reynolds Number and Geometry Variations on Airfoil Performance:

The effects of operating a very low Reynolds numbers and several airfoil geometry parameters have been investigated using the INS2D code and various members of the NACA 4-digit airfoil family. The geometry definitions for these airfoils are parameterized for maximum thickness, maximum camber, and location of maximum camber. A wide range of parameter variations is possible and section coordinates are easily generated. In addition, there is a large body of experimental performance data available for many members of this airfoil family. Although the majority of this data is at much higher Reynolds numbers, it provides a useful reference point for discussions of section performance at very low Reynolds numbers.

Reynolds Number:

The most obvious effect of operation at very low Reynolds numbers is a very large increase in the section drag coefficients. In the $Re\ 10^3$ operating range the drag increases a full order of magnitude. Zero lift drag coefficients for airfoils range from 300 to 800 counts depending on the Reynolds number and geometry. These high drag values are in line with theoretical laminar plate drag, which is inversely proportional to the square root of the Reynolds number.

The increase in drag is unfortunately not reciprocated in lift. Lift coefficients remain of order one, resulting in a large reduction in the L/D ratios. Flight at these Reynolds numbers is much less efficient than at higher Re and available power is a limiting technological factor at very small scales. It is important to operate the airfoil at its maximum L/D operating point, but this requires operating very close to the maximum steady-state lift coefficient. Even small increases in the maximum lift coefficient are significant and generally translate to higher L/D ratios.

Flow at these low Reynolds numbers is viscously dominated, and as the Reynolds number is reduced, the effects of increasing boundary layer thickness become more and more pronounced. The definition of 'boundary layer' at such low Re in a fully viscous flow field is an inexact notion. Here it is generalized as the low velocity flow adjacent to the body over which the pressure gradient perpendicular to the surface is close to zero. Regions of constant pressure extend a significant distance away from the actual surface of the airfoil and the effective geometry is significantly altered by the presence of the boundary layer.

Unlike the very thin viscous layers held close to the geometry at much higher Re , in this operating regime the boundary layer has a dramatic effect on surface pressures, closer to that of a separation streamline. This can be demonstrated by considering the inviscid and viscous pressure distributions on an NACA 0008 at zero angle of attack. This is shown in Figure 5. Both the $Re\ 6000$ and $Re\ 2000$ cases are fully attached. As the Re is reduced, the value of the minimum pressure and the slope of the adverse gradient in the pressure recovery are reduced. This weakened pressure recovery does impact the pressure drag, but at an angle of attack, the largest effect is on lift. Figure 6 is a similar plot for the NACA 0002. Here again, all three cases are fully attached. For this 2% thick section, there is essentially no recovery of pressure in the $Re\ 1000$ case. It behaves as if predominately separated. Also of note is the small increase in the magnitude of the minimum pressure. This is due to the effective thickening of the section. This region of the pressure distribution is smoothed and shifted aft. This has an important effect on the maximum attainable lift coefficient.

Viscous effects alleviate and smooth the high gradients present in the nose region of an airfoil. The reduction in the height of the leading edge suction peak and the reduction in slope of the adverse pressure recovery gradient delay the onset of separation and stall. Leading edge separation is delayed in thin sections, and trailing edge separation is delayed in thicker sections. The results are higher attainable angles of attack and higher maximum steady-state lift coefficients. Pressure distributions for a NACA 0008 airfoil at two degrees angle of attack are

presented in Figure 7. The Re 6000 case is on the verge of T.E. separation, but the Re 2000 case does not separate until 3.5 degrees. Lift coefficients for the two cases agree within 3.5%. The Re 2000 case achieves the same amount of lift with a much weaker suction peak, a less adverse recovery gradient, and an additional margin of separation-free operation.

Reynolds number affects the lift curve by reducing the slope in the linear range, but also extending the linear range to higher angles of attack. The linear lift range is generally characterized by fully attached flow at the trailing edge. While operating within this range, the displacement effect of the boundary layer progressively reduces the effective camber of the section with increasing angle of attack. The change in effective geometry is greater at lower Reynolds number. The delay in separation with reduced Re extends the linear range to higher angles of attack. Beyond the linear lift range, the reduction in lift curve slope becomes less pronounced as the Reynolds number is lowered. Once the flow does separate, growth of the separated region is delayed by a reduction in Reynolds number. The overall effect is a significant increase in both the maximum steady-state angle of attack and lift coefficient.

Lift curves for a NACA 0002 and a NACA 0008 are presented in Figure 8. The calculations are at Re 2000 and Re 6000. The reduction of slope is most apparent for the 0002 airfoil, but both sections exhibit the extension of the linear lift range. The 0002 section remains linear across its entire operating range; this section does not separate from the trailing edge. Its flow field becomes unsteady due to leading edge separation. The Re 2000 case reaches 5.5 degrees and a lift coefficient a full tenth greater than the Re 6000 case. Similar gains occur for the 0008 section at Re 2000 and for this section the effects of Reynolds number on the non-linear portion of the lift curve are clearly depicted.

Trailing edge streamlines for the 0008, at Re 2000 and Re 6000, are provided in Figures 9 and 10. The plots begin at the upper edge of the linear lift range for each Re. All of the streamline seeds are identical in both figures and the point of separation is indicated. The onset of T.E. separation is pushed from 2 degrees at Re 6000 to 3 degrees at Re 2000. As the angle of attack is increased, the differences in performance grow; the lower Re case achieves more than two degrees higher angle of attack for similar amounts of T.E. separation.

There is a basis for low Reynolds number lift recovery in both theory and experiment. Thwaites' laminar boundary layer theory indicates that for the same velocity distribution, the separation criterion becomes more critical proportional to the Reynolds number. Based on this alone, a reduction in Re would be hasten laminar separation, but the separation criterion is also proportional to the local velocity gradient and an integral function of the local velocity. For these airfoils, operating at very low Reynolds numbers, the displacement effects of the boundary layer that accompany the reduction of Reynolds number appear to dominate and separation is delayed. The experimental work of Thom and Swart⁵ consisted of testing small a R.A.F. 6a airfoil model in an oil channel and water channel at Reynolds numbers below 2000. They observed large increases in lift at fixed angles of attack as the Reynolds number was reduced from 2000 towards a value of one.

Airfoil efficiency is reduced as Re is decreased due to the drag rise, but this lift recovery is significant for applications where the available power is not severely constrained. Current

technology would require the use of an external power source, but in the future, technological developments should allow for higher energy storage capacities for very small devices. This result implies that as vehicles become smaller they should be more capable of generating sufficient lift, albeit at a large cost in energy expenditure.

Maximum Section Thickness:

The effect of maximum thickness variations are investigated using uncambered NACA 4-digit airfoils ranging from 2% to 8% thick in 2% increments. Performance estimates for each section were computed at Re 6000 and Re 2000. Airfoil thickness variations appear to have two principal performance effects. A drag penalty, due to the pressure recovery attributable to increased thickness, is to be expected, but a strong reduction in the lift curve slope is also an effect of increasing thickness. The apparent trends in drag are consistent with behavior at higher Reynolds numbers, but the magnitude of the variations are markedly increased. Behavior in lifting performance is significantly different, with increasing thickness resulting in a severe performance penalty.

Effect of Thickness on Drag:

The variations in drag with section thickness are illustrated by the airfoil drag polars in Figure 11. It is interesting to compare the calculated values with airfoils of the same family operating at higher Reynolds numbers and with the drag of a fully laminar flat plate. The experimental data for the NACA 4-digit family is taken from Abbot and Von Doenhoff⁶ at Re 6 million. Over the practical range of section thickness and for a fixed Reynolds number, the relationship for this family of airfoils between maximum thickness and the zero lift drag is well approximated by a linear function. The effect of thickness variations on the zero lift drag may then be expressed as a reference zero thickness drag and a slope. The reference values and slopes are provided in Table 1. The laminar plate drag is also included for comparison.

The most obvious results are a general consequence of operation at very low Reynolds numbers. The drag coefficients are a full order of magnitude greater, but the lift coefficients are of the same order as at more conventional Reynolds numbers. This results in very low section lift to drag ratios of order one as opposed to order 100. Also notable is the large increase in the drag coefficient, nearly doubled, between the Re 6000 and Re 2000 results. In this regime, small magnitude changes in Re result in quite large variations in the drag coefficient. The laminar flat plate drag mimics these trends and provides a very good estimate the zero lift, zero thickness airfoil drag for the low Re values. The laminar flat plate drag differs only by 5.3% at Re 6000 and 9.5% at Re 2000. This result is not surprising considering that the zero thickness reference *is* a flat plate. This supports the assumption of a linear relationship between thickness and zero lift drag for these airfoils.

The slopes of the drag penalty associated with increasing thickness are seen to increase with decreasing Reynolds number, but the rates of drag increase relative to the zero thickness drag are similar. Across the three cases, there is a reduction from 4% to 2% between Re 6 million

and Re 6000, and a very slight reduction from Re 6000 to Re 2000. There appear to be few surprises when considering the zero lift drag of these sections and the effect of maximum section thickness at these low Reynolds numbers. Although the magnitudes of the drag coefficients increase dramatically, they are in line with simple laminar plate results. The variations with thickness also exhibit an order of magnitude increase, but the trends in the behavior are consistent with those at higher Reynolds numbers.

Effect of Thickness on Lift:

The effects of increased thickness on lift performance are a reduction in the lift curve slope within the linear range and a more rapid reduction in lift curve slope in the non-linear range. These two features are apparent in the lift curve slopes of Figures 12 and 13 for Re 6000 and Re 2000 respectively. Within the linear range, the inviscid lift curve slope of an airfoil benefits from increased thickness, with thicker sections obtaining as much as a 10% increase in lift curve slope over the thin airfoil value of 2π per radian. At more conventional Reynolds numbers, 10^6 and higher, viscous effects then degrade the lift curve slope, with the end result of lift curve slopes 5% to 10% below the thin airfoil value. The increased thickness of the upper surface boundary layer relative to the lower surface boundary layer at angle of attack effectively reduces the camber of the airfoil. The inviscid gains and viscous losses are generally seen to cancel resulting in lift curve slopes close to 2π per radian across a range of section thickness. This is not the case for Re of order 10^3 .

In this range of operation, the viscous boundary layer growth dominates and increasing thickness results in a significant decrease in lift curve slope in the linear range. The lift curve in Figure 12 shows as much as a 35% reduction in lift curve slope for the 8% thick section. The 2% sections come closest to the thin airfoil value, showing a 15% reduction. The effect of reducing the Re from 6000 to 2000 is a further reduction in the slope for all but the thickest section. The 2% section shows the greatest effect with a 5.2% reduction due to Re effects, with a decreasing effect with increasing thickness. The 8% section appears to be unaffected within the linear range.

The decambering effect of the increased boundary layer thickness is easily visualized by considering constant velocity contours in the flow field. The area of reduced flow velocity is quite large and the validity of defining a reference edge value is debatable, but the contours chosen are at a fixed fraction of the free stream velocity, low enough to be considered within the boundary layer. This provides a qualitative notion of the boundary layer geometry.

Several $0.2V_\infty$ contours are drawn for the 0002 and 0008 sections at Re 6000 in Figure 14. This velocity represents a region far within what might be considered as the boundary layer. The region of low velocity flow associated with the airfoil surface extends considerably farther out into the flow field. Three angles of attack, zero, two, and four degrees are indicated. These represent the zero lift condition, the upper limit of the linear lift range for the 0008, and a point within the non-linear range, where trailing edge separation comes into play. The boundary layer has little effect on the effective geometry of the 0002 airfoil, but the thicker upper surface boundary layer of the 0008 significantly decreases the effective camber of the airfoil.

For both Re values, the effect of increasing thickness appears to be a more rapid reduction in the lift curve slope once past the linear lift range. The effect is reduced at the lower Reynolds number and the linear range is effectively extended to higher angles of attack as described earlier. The trailing edge streamlines for the 0002 at Re 6000 are shown in Figure 15. The equivalent plot for the 0008 was presented as Figure 9. These plots begin at 2.0 degrees angle of attack, at the edge of the 0008's linear range. The 0002 is fully attached up to stall. The 0008 is almost fully attached at 2.0 degrees, with visible T.E. separation at 95% chord, but by 3.0 degrees there is significant separation at 75% chord. This moves to 60% at 4.0 degrees. These separated regions result in a large displacement of flow within the aft boundary layer increasing the decambering effect and resulting in the larger reductions in lift compared to the fully attached 0002 airfoil.

Effect of Camber:

If thickness variations have such a significant impact on airfoil behavior, what else may be done to enhance the performance of a given section? Is the design space at these very low Reynolds numbers varied and complex, or is a flat plate as good or better than anything else? Consideration of camber, its magnitude and placement, is a logical step in the investigation of these questions. The introduction of camber does offer the potential for significant performance gains over a simple flat plate. The effects of camber do not differ significantly from those at much higher Reynolds numbers, but the fact that the detailed geometry is still an important and effective driver of performance at such low Reynolds numbers is itself a useful conclusion.

A comparison of NACA 0002 and 4402 sections indicates the gross effects of camber on performance. Lift curves and drag polars are provided for Re 1000, 2000, and 6000 in Figures 16 and 17. As at higher Reynolds numbers, the first order effect on the lift curve is seen as a translation to the left with increasing camber. The addition of 2% camber results in a 2.0 to 2.5 degree shift in the zero lift angle of attack. The maximum achievable steady-state lift coefficients also increase. In the case of these two sections, there is a 30% increase in the maximum steady-state lift coefficient. Increases of less than one tenth in C_l are still very significant due to the very low lift to drag ratios seen under these conditions. Although the drag also increases, in this regime the ability to attain higher lift coefficients generally results in net gain in lift to drag ratio. Due to the introduction of camber, the maximum lift to drag ratio increases from 4.5 to 5.4 at Re 1000 and from 9.3 to 11.0 at Re 6000.

Within the linear range, the reduction in lift curve slope with decreasing Reynolds number is visible for the 0002, but the effect of reducing Re on the 4402 is different. It appears as a drift to the right in α_{ZL} as the reduction in Re uniformly reduces the effective camber of the section across the entire linear lift range. All but the Re 1000 case eventually suffer from leading edge separation, but the onset is delayed slightly, most likely attributed to the increase in the ideal angle of attack that comes with the introduction of camber. The Re 1000 case appears to become unsteady due to a large degree of T.E. separation.

The delay in trailing edge separation attributed to reducing Reynolds number is also visible in the 4402 results. At five degrees, the Re 6000 case separates at 55% chord while the Re 2000 case separates at 92% chord. The Re 1000 case is still fully attached at this point, and at 7.5 degrees is still attached up to 65% chord. Consideration of the drag polars in Figure 17 reveals trends very similar to those at higher Reynolds numbers. The addition of camber results in an increase in zero lift drag and an upward shift of the polars towards higher lift coefficients.

Encouraged by the effectiveness of camber in this single instance, further analyses have been completed to investigate the possible benefits of varying the magnitude and distribution of camber. The design space is explored using 9 airfoils spanning 2% to 6% maximum camber located at 30%, 50%, and 70% chord. All of the sections are 2% thick NACA 4-digit profiles. All calculations were completed at Re 12000.

The lift curves provided in Figures 18 are for 2% and 4% camber at all three of the chord locations. In both plots, the aft shift of maximum camber results in a less severe reduction of lift past the linear range, higher attainable lift coefficients, and higher lift to drag ratios. This correlates with reduced trailing edge separation for a given angle of attack. The aft cambered sections exhibit separation at a lower angle of attack due to the steep adverse gradient near the trailing edge, but the extent of separation grows very slowly with increased angle of attack. As the angle of attack rises, the majority of the low-pressure side experiences less adverse gradients than a similar section with forward camber. The effect on separation is to contain it aft of the maximum camber location by maintaining less adverse gradients ahead of it. This functions like a separation ramp in the pressure distribution.

Comparison of the L/D ratios of the nine sections begins to reveal the complexity present in this design space that is so common in airfoil design. Although the additional camber reduces α_{ZL} , separation begins to appear at about the same lift coefficient and is more severe in the 4% camber cases. Only the aft position of the 4% camber cases manages to out perform the 2% camber cases. The other two are lower in L/D and roughly equivalent in lift coefficient. The maximum L/D ratios for all nine airfoils are provided in Table 2. The 6% camber cases, which are not shown, exhibit even earlier and more aggressive T.E. separation.

The effects of varying the amount of camber, while fixing the location at the 70% chord location, is depicted in Figure 19. The increase in camber causes a non-linear penalty in drag for a given lift coefficient, but this is tempered by the ability to attain higher lift coefficients. For these three cases, the maximum L/D is attained by the 4% camber section. The effects of varying the location of maximum camber for a fixed 4% camber is depicted in Figure 20. The aft movement of camber results in significantly higher drag below $C_l=0.45$, but this geometry is able to achieve higher lift coefficients within the steady-state operating limitation. It is unlikely that one would be operating a section at low lift coefficients, since the L/D ratios are greatly reduced at low angles of attack.

This simple 9-point test matrix indicates that aft camber is beneficial. Selection of the amount of camber is less clear, but for this particular camber definition, it should lie in the midrange of the values considered. This study of camber variations is not meant to be a detailed indicator for design. The camberline is rather rigidly defined and the sampling is sparse. It is,

however, indicative of the large variations in performance that exist within the design space and some of the physical trends responsible.

¹ Rogers, S. E. and Kwak, D., "An Upwind Differencing Scheme for the Steady-state Incompressible Navier-Stokes Equations," NASA TM 101051, November 1988.

² Rogers, S. E. and Kwak, D., "An Upwind Differencing Scheme for the Time Accurate Incompressible Navier-Stokes Equations," *AIAA Journal*, Vol. 28, No. 2, February, 1990, pp. 253--262.

³ Chorin, Alexandre Joel, "A Numerical Method for Solving Incompressible Viscous Flow Problems," *Journal of Computational Physics*, Vol. 2, No. 1, 1967.

⁴ Drela, M., Giles, M. B., "ISES - A Two-Dimensional Viscous Aerodynamic Design and Analysis Code," AIAA Paper 87-0424, AIAA 25th Aerospace Sciences Meeting, Reno, NV, January 1987.

⁵ Thom, A., Swart, P., "The Forces on an Aerofoil at Very Low Speeds,"

⁶ Abbot, Ira H. and Von Doenhoff, Albert E., *Theory of Wing Sections*, Dover Publications Inc., New York, 1959.

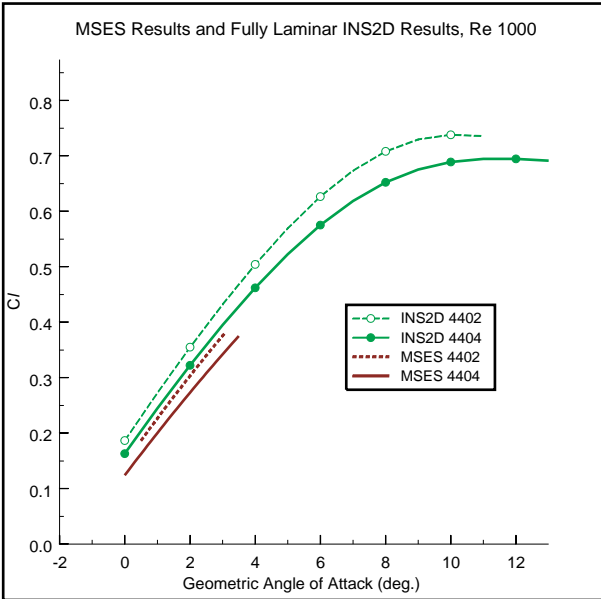


FIGURE 1

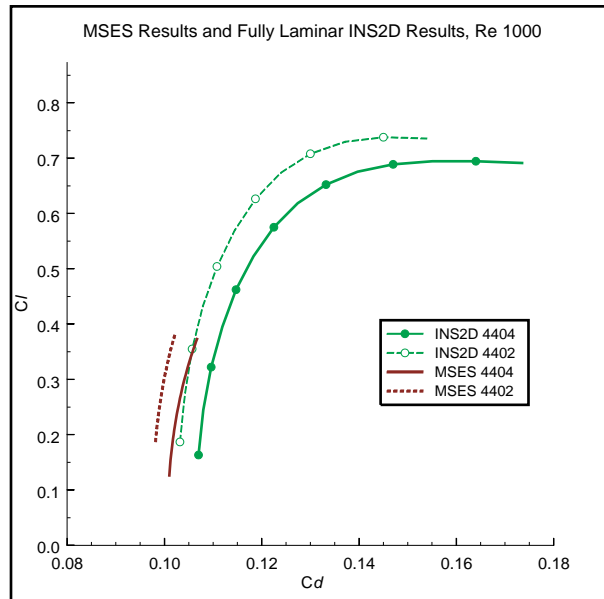


FIGURE 2

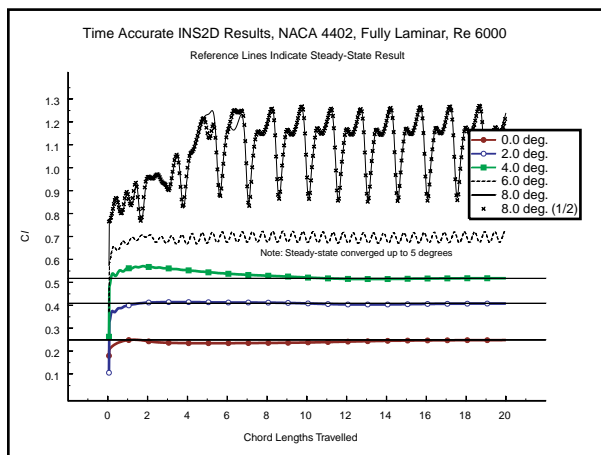


FIGURE 3

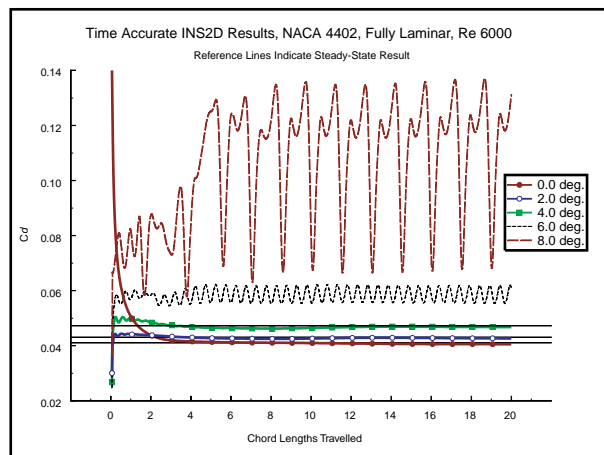


FIGURE 4

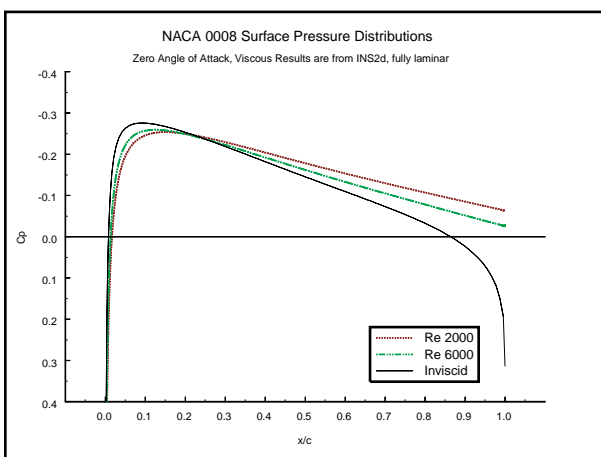


FIGURE 5

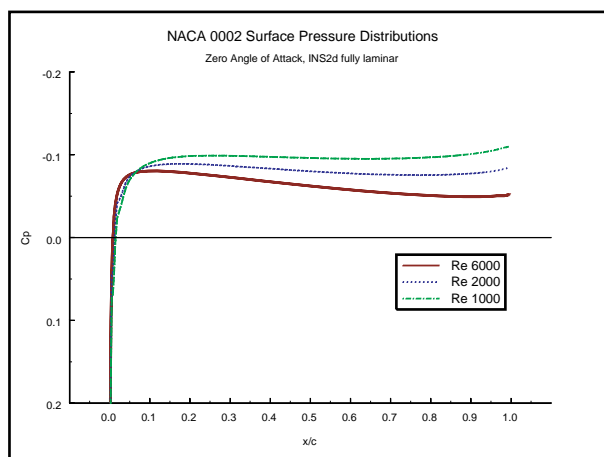


FIGURE 6

NACA 0008 Pressure Distributions

$\alpha=2.0$ degrees, Re 2000 and Re 6000, INS2d Fully Laminar

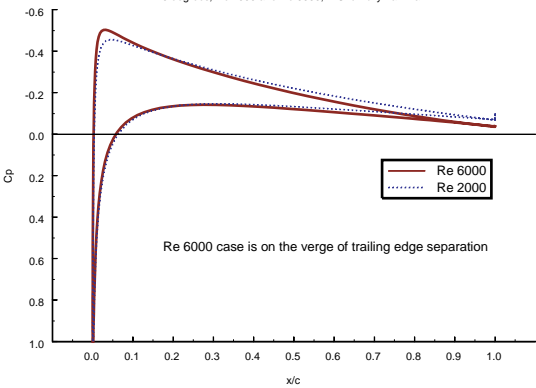


FIGURE 7

Lift Curves for the NACA 0002 and NACA 0008

Re 2000 and Re 6000, INS2d Fully Laminar

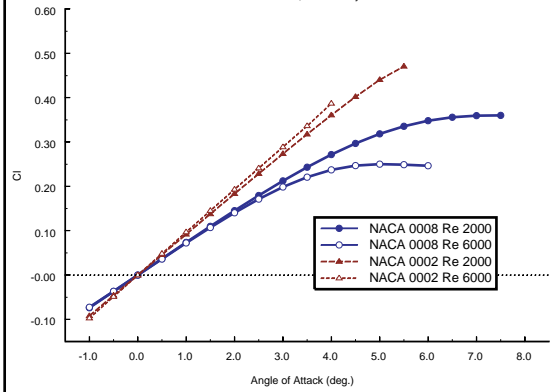


FIGURE 8

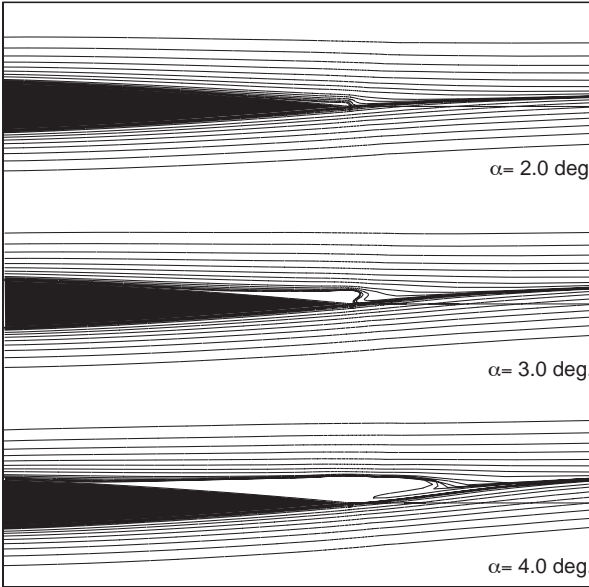


Figure 9. Aft Streamlines for the NACA 0008 at Re 6000 at three angles of attack. Aft 45% of airfoils is visible.

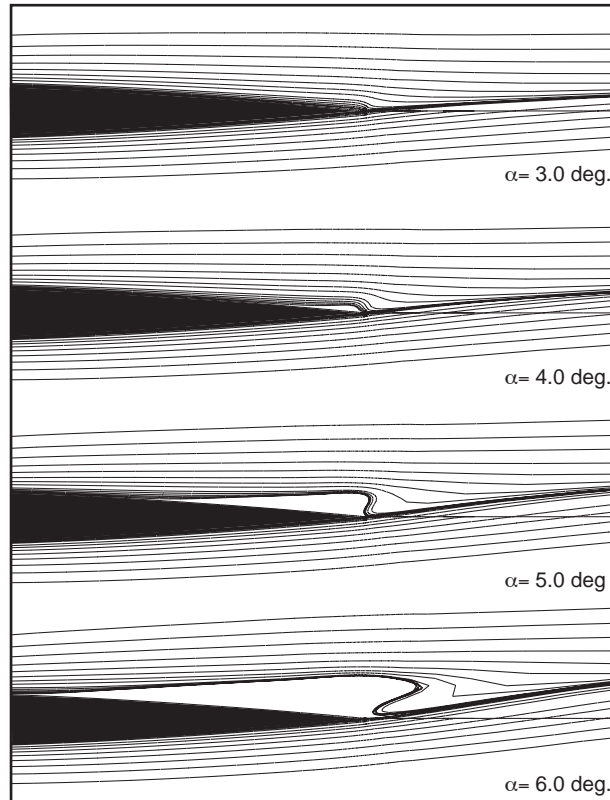


FIGURE 10 (RE 2000)

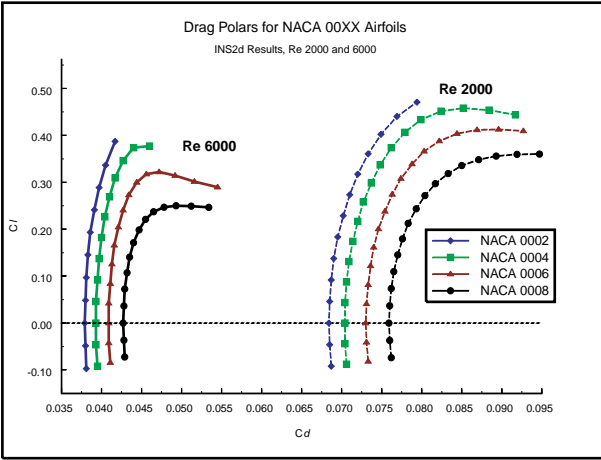


FIGURE 11

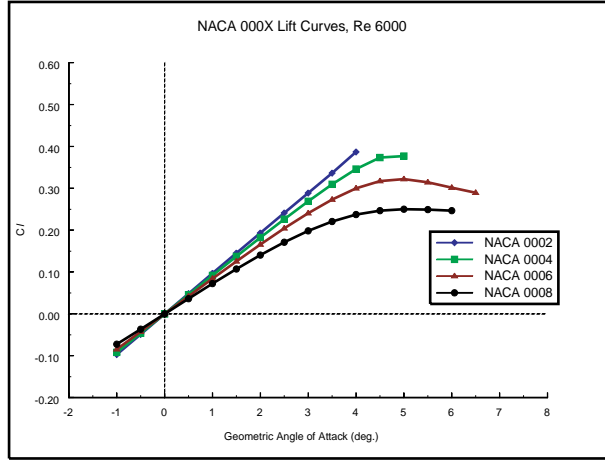


FIGURE 12

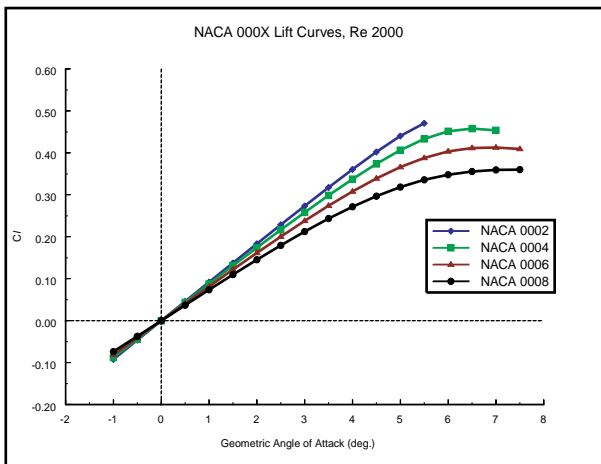


FIGURE 13

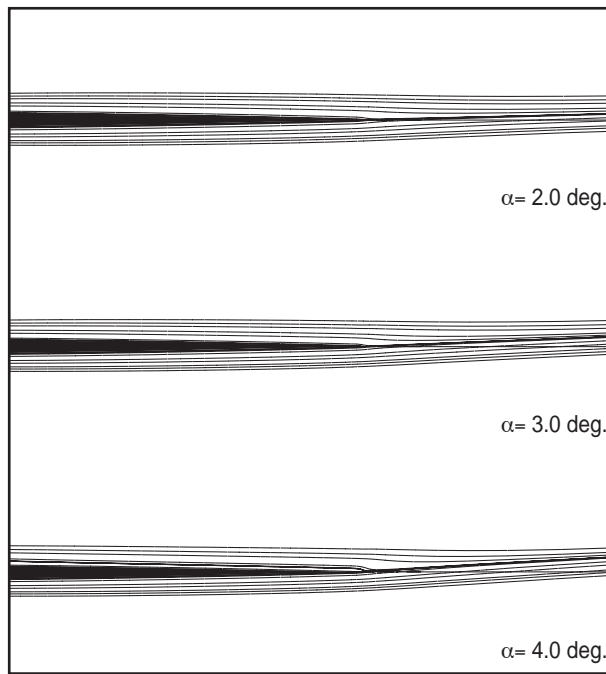


FIGURE 15

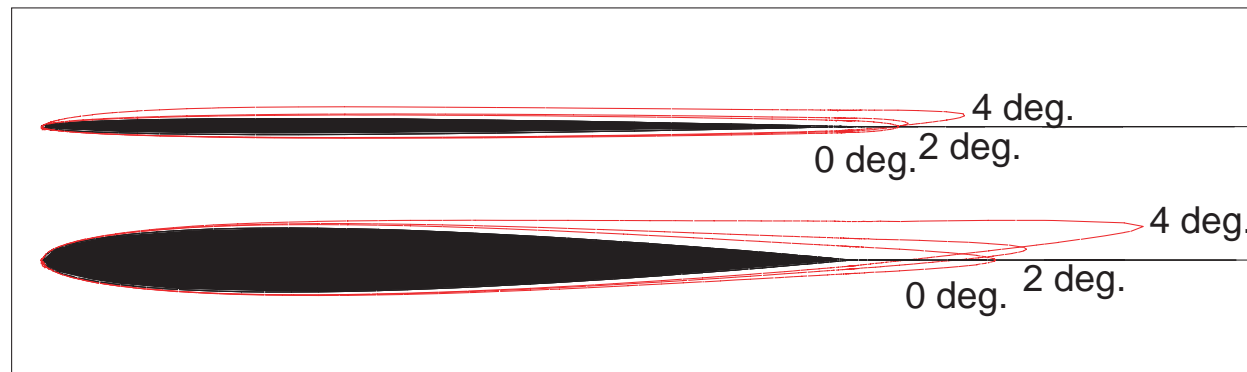


FIGURE 14

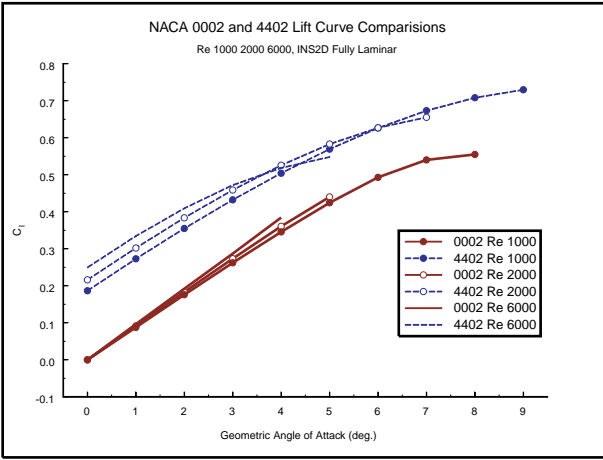


FIGURE 16

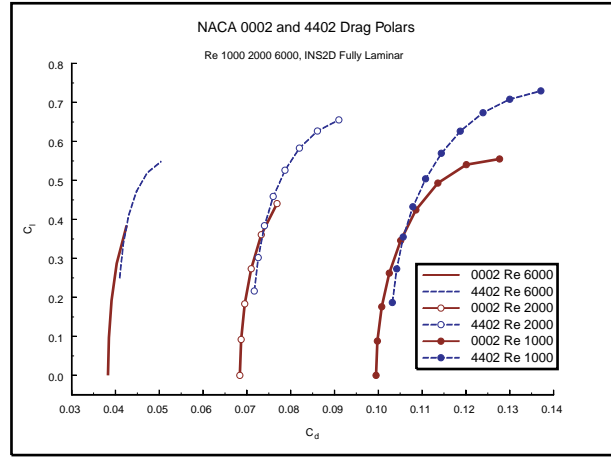


FIGURE 17

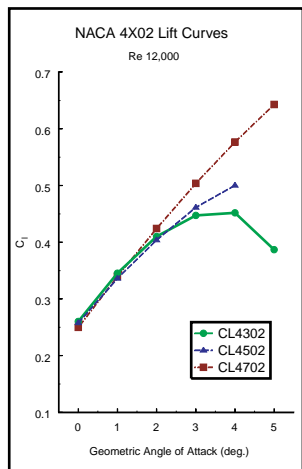
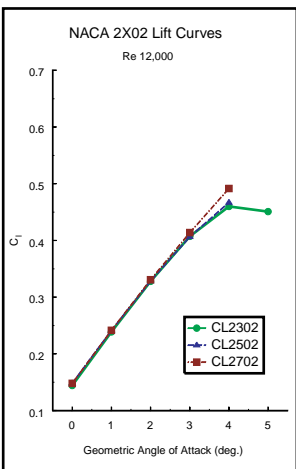


FIGURE 18

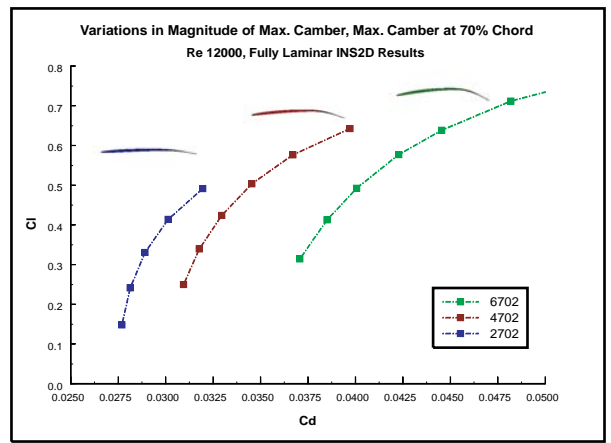


FIGURE 19

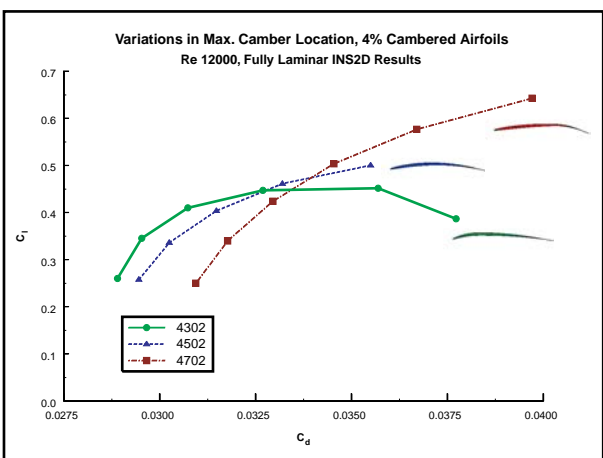


FIGURE 20